JOURNAL OF AIRCRAFT
Vol. 42, No. 5, September–October 2005

Nose Bluntness for Side-Force Control on Circular Cones at High Incidence

Rajan Kumar* and P. R. Viswanath†
National Aerospace Laboratories, Bangalore 560 017, India
and
O. N. Ramesh‡
Indian Institute of Science, Bangalore 560 012, India

An experimental investigation has been carried out to study the effect of nose bluntness on the characteristics of vortex asymmetry and induced side forces on slender cone models at low speeds. Two cone models with semi-apex angles of 8 and 12 deg were utilized, and on each model nose bluntness was varied up to 20% (based on base diameter). Measurements made consisted of six-component balance loads over a wide range of Reynolds number from 0.4×10^6 to 5.4×10^6. The results show that the onset of vortex asymmetry with nose blunting correlates with geometrical parameters and is practically independent of Reynolds number. The (maximum) side-force levels decrease initially up to a certain bluntness ratio, then increase, followed by a gradual decrease for large values of bluntness ratios. This decrease or increase in side-force levels with nose blunting is associated with a corresponding increase or decrease, respectively, in the onset of vortex asymmetry. Whereas the increase in side-force level beyond the first minimum is qualitatively similar to that observed in earlier studies, the present data definitely indicate that there is a progressive decrease in side-force levels to relatively low values for large bluntness ratios, which could form an important design input. The bluntness ratio corresponding to the occurrence of the first minimum in (maximum) side force depends on the cone angle and is nearly independent of Reynolds number.

Nomenclature

A_b	=	base area, $\pi/4D^2$
C_N	=	normal force coefficient, normal force$/(q_\infty A_b)$
C_p	=	static pressure coefficient, $(p - p_\infty)/q_\infty$
C_S	=	side force coefficient, side force$/(q_\infty A_b)$
D	=	base diameter, 160 mm
M_∞	=	freestream Mach number
p	=	local static pressure
p_∞	=	freestream static pressure
q_∞	=	freestream dynamic pressure
Re_D	=	freestream Reynolds number based on base diameter D
r_N	=	nose radius
α	=	angle of incidence
α_{onset}	=	angle for the onset of vortex asymmetry
θ_c	=	semicone angle
ϕ	=	roll angle

Introduction

MODERN fighter aircraft and missiles are expected to perform poststall maneuvers to achieve tactical advantages. This results in flight at high angles of attack (up to 45–50 deg), and knowledge of the nonlinear aerodynamics including strong viscous effects leading to crossflow separation become very important in the design of a flight vehicle. One of the important problems, which has received considerable attention during the last two decades, is the phenomenon of vortex asymmetry on pointed forebodies at high angles of attack and the resulting side forces and adverse yawing moments even in symmetric flight (zero side slip).[1–4] The yawing moments generated are too large to be controlled by the use of the rudder power in the case of a fighter aircraft. The major geometric parameters that are known to influence vortex asymmetry include nose apex angle, forebody cross-sectional shape, and fineness ratio of the slender body. The side forces generated are strongly Reynolds number dependent, and the effects gradually decrease with an increase in flight Mach number. The problem is essentially predominant at low to subsonic speeds in which regime high alpha maneuvers normally occur.

Because the magnitude of side forces and adverse yawing moments generated are large and cannot be easily controlled, there have been several attempts to reduce and possibly eliminate the asymmetric forces and moments by forcing the flow into a symmetric vortex configuration using both passive and active techniques. Some of the passive devices that have been tried include nose blunting,[5–9] forebody strakes,[10–14] nose booms,[12,15] deployable strakes,[16] and a variety of boundary-layer trips.[7,17,18] Most of the previous studies have been exploratory in nature, and the benefits have been demonstrated over a limited range of flow parameters. Some of the active techniques explored include nose rotation[19] and rotating strakes.[10]

Nose blunting is a simple and viable device, and it can have strong relevance in the design of combat aircraft, missiles, and projectiles. Limited studies[5–8] on this problem have shown that nose blunting delays the onset of vortex asymmetry and lowers the (maximum) side-force levels; these benefits have been demonstrated over a limited range of flow parameters. The primary effect of nose blunting is probably that it prevents the formation of the initial, well-defined, conical type of asymmetry that occurs with a sharp tip. Figure 1 (reproduced from Ref. 1) shows the summary of data available in dealing with nose bluntness on pointed forebodies, and very little work appears to have been done in the last decade. Maximum side-force levels show an initial decrease up to a certain bluntness ratio, which is followed by a rise for larger bluntness ratios. The optimum bluntness ratio (nondimensionalized by the base diameter) seems to vary depending on the overall slenderness ratio of the body. Several interesting questions remain both from a scientific as well as from a design application point of view: these include 1) what the

Presented as Paper 2004-0037 at the AIAA 42nd Aerospace Sciences Meeting and Exhibit, Reno, NV, 5–8 January 2004; received 21 April 2004; revision received 21 August 2004; accepted for publication 21 August 2004.

*Scientist, National Trisonic Aerodynamic Facilities. Member AIAA.
†Head, Experimental Aerodynamics Division. Associate Fellow AIAA.
‡Assistant Professor, Department of Aerospace Engineering.

REFERENCE	L_N/D	L/D	NOSE SHAPE	M_o	$Re_D \times 10^6$	α
○ 5	3.5	3.5	OGIVE	0.25	0.8	50^o
□ 6	3.0	8.0	OGIVE	0.6	0.2	α_{MAX}
△ 7	3.5	3.5	OGIVE	0.25	0.8	α_{MAX}
▽ 8	3.5	3.5	20^o CONE	0.25	1	α_{MAX}

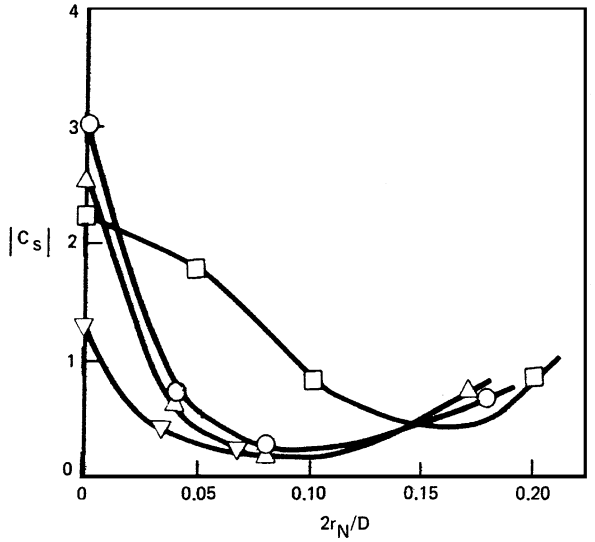

Fig. 1 Effect of bluntness on side force coefficient (Ref. 1): D = base diameter, L = overall length, and L_N = nose length.

scaling parameter is for the nose diameter, 2) what the causes of the second rise in side force levels beyond the optimum bluntness ratio are, and, finally, 3) what the Reynolds number and Mach number effects are on the effectiveness of nose blunting and the optimum nose bluntness ratio.

In this paper, the effects of nose blunting for side-force alleviation are addressed in significant detail through a systematic parametric study. Experiments have been carried out on two cone models of semi-apex angles 8 and 12 deg, covering a wide range of Reynolds numbers (based on the base diameter) from 0.4×10^6 to 5.4×10^6 at low speeds. On each cone model, the nose bluntness ratio ($2r_N/D$) was varied from 0% (sharp cone) up to 20% (based on the base diameter). Accurate six-component balance measurements have been made over the incidence range from 0 to 45-deg. Surface pressure distributions on the 12-deg cone model have been made to gain a better understanding of crossflow features and bluntness effects. Surface flow visualization studies have been carried out to provide information on the structure of the crossflow separation, including the type of separation (laminar, transition, or turbulent). The paper contains detailed discussion on the aspects of vortex asymmetry onset and on side-force generation with Reynolds number and crossflow features as influenced by nose bluntness.

Experiments

Test Facilities

A major part of the experiments was carried out in the National Aerospace Laboratories (NAL) 1.2×1.2 m trisonic wind tunnel to take advantage of a wide range of Reynolds numbers possible in the facility by varying both freestream Mach number and tunnel stagnation pressure. A large part of the measurements was carried out in this test facility. Limited experiments involving balance and surface pressure measurements at the lowest freestream velocity (40 m/s) were carried out in the NAL 1.5×1.5 m low-turbulence, low-speed wind tunnel. In both facilities, the incidence range of 0–45 deg was carried out by employment of a high alpha attachment integrated to the main pitch system.

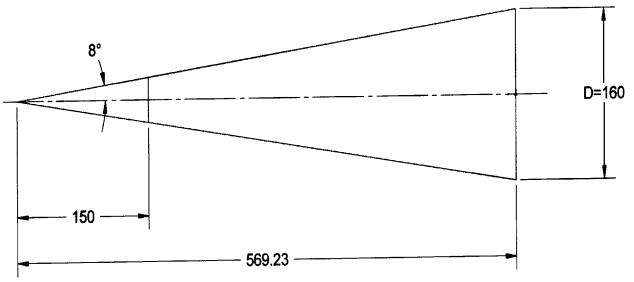

r_N, mm	0	1.6	3.2	5.6	8	12	16
$2r_N/D$, %	0	2	4	7	10	15	20

All dimensions are in mm

Fig. 2 Geometrical details of 8-deg cone model.

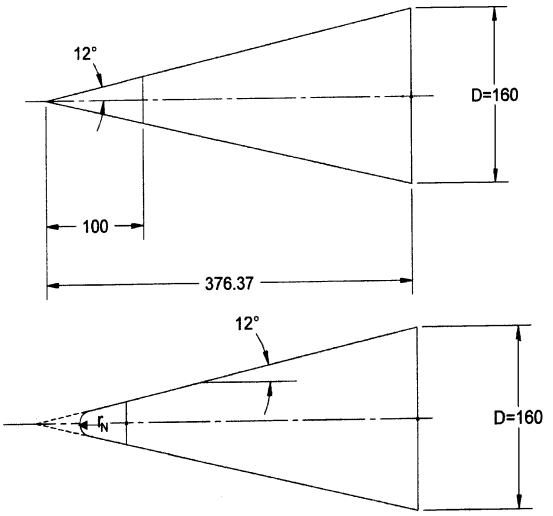

r_N mm	0	2.4	4.8	7.2	9.6	12	14.4	16.8
$2r_N/D$, %	0	3	6	9	12	15	18	21

All dimensions are in mm

Fig. 3 Geometrical details of 12-deg cone model.

Test Models

Measurements were made on two cone models with semi-apex angles of 8 and 12 deg, each with a base diameter of 160 mm (Figs. 2 and 3). Each cone model was made in two sections: the front portion with either a sharp cone tip or a blunt nose (with different nose radii) and the rear (cone–frustum) portion that was the same for a given cone model. There was also a provision to roll the front nose portion at a 45-deg interval, which was very convenient for assessing the roll sensitivity in the experiments. Nose radius was varied from zero (sharp cone) to 16 mm on the 8-deg cone (Fig. 2) and 16.8 mm on

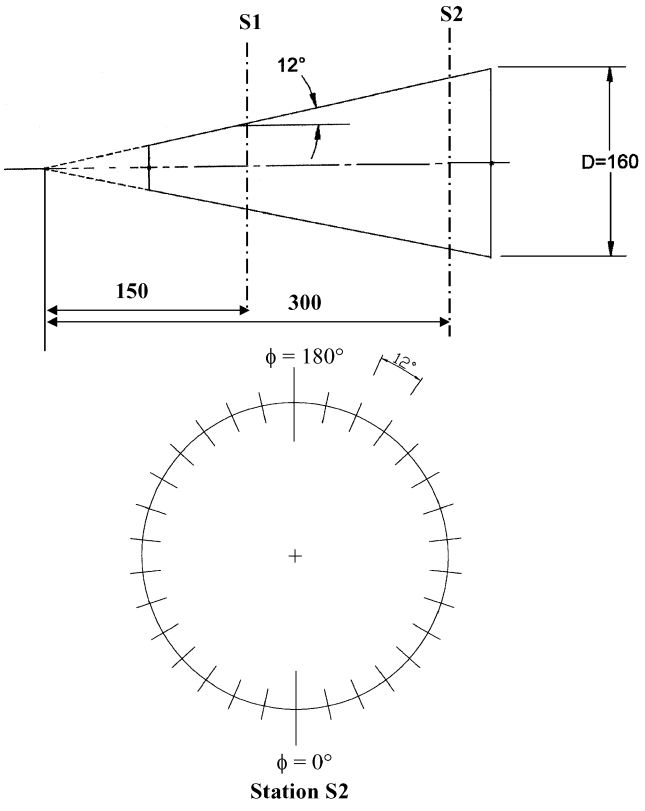

Fig. 4 Geometrical details of 12-deg cone pressure model.

the 12-deg cone (Fig. 3), providing nose bluntness ratios (based on base diameter) of up to 20 and 21%, respectively. Static pressure measurements were made on the 12-deg cone model (Fig. 4). For this purpose, another rear portion of the model was fabricated and instrumented with two rows of static pressure taps (30 numbers each at the $S1$ and $S2$ stations), as shown in Fig. 4.

Measurements and Instrumentation

1) Strain-gauge balance measurements were made for both pointed as well as blunted cone models in the incidence range of 0–45 deg. Two separate internal strain-gauge balances of appropriate ranges were used in the 1.2- and 1.5-m wind tunnels so that data accuracy is maintained. The load ranges for the 38.1-mm (1.5-in.), six-component strain-gauge balance used in the 1.2-m wind tunnel are normal force = 545 kg, side force = 273 kg, axial force = 27 kg, pitching moment = 42 kg · m, yawing moment = 17 kg · m, and rolling moment = 4.62 kg · m. The load ranges for the five-component balance used in the 1.5-m low-speed tunnel are normal force = 8 kg, side force = 4 kg, pitching moment = 0.9 kg · m, yawing moment = 0.45 kg · m, and rolling moment = 0.05 kg · m. Side-force measurements were made using the side-force element of the balance in both cases.

2) Static pressure distributions (around the model circumference) were measured on the 12-deg cone (Fig. 4) for the pointed and a few selected blunt nose configurations in the low-speed wind tunnel. All of the static pressure tubes were connected to two units of 48-port pressure scanners, coupled to micromanometers of a ±200-mm range of water.

3) Surface flow visualization studies using titanium-dioxide in oil were carried out on selected model configurations to assess both symmetric and asymmetric vortex flow features.

Test Conditions

For the tests in the 1.2-m tunnel, Reynolds number (based on the base diameter, Re_D) was varied in the range of 0.9×10^6 to 5.4×10^6 by operating the tunnel in the Mach number range of 0.17–0.40 and by varying the tunnel stagnation pressure in the range of 138 kN/m^2 (20 psi) to 414 kN/m^2 (60 psi). This large range of Re_D was utilized to establish Reynolds number effects both on vortex asymmetry onset as well as side-force generation, which are both very important in design applications. Also note that the compressibility effects may slightly reduce[20] the maximum side-force levels (about 2–3% between $M_\infty = 0.3$ and 0.4).

The measurements at the lowest Reynolds number, $Re_D = 0.4 \times 10^6$, was obtained in the NAL 1.5×1.5 m low-speed wind tunnel at a freestream velocity of 40 m/s; the balance measurements were carried out in a pitch and pause mode in steps of 2 deg at a sampling rate of 50 samples/s for a time period of 10 s. In the 1.2-m tunnel, data were obtained at continuous pitch mode at a slow rate of 2 deg/s with a sampling frequency of 275 Hz; it was ascertained that side forces generated in the continuous pitch and pitch/pause mode were virtually the same. The balance and transducer outputs signals were acquired on a personal-computer-based data acquisition system and processed offline on a computer.

Measurement Uncertainties

The accuracy of the measured force and moment coefficients depends on the individual accuracy of various measuring instruments used and on the flow parameters. The strain-gauge balances and pressure transducers were accurately calibrated before use in the present experimental program. The measurement accuracy of strain balance is ±0.1% of full capacity. The uncertainty obtained by static calibration of pressure transducers is ±0.5% of full scale. Based on the method suggested by Kline and McClintock[21] and taking into account the repeatability of tests, estimates of maximum measurement uncertainty were determined and are as follows:

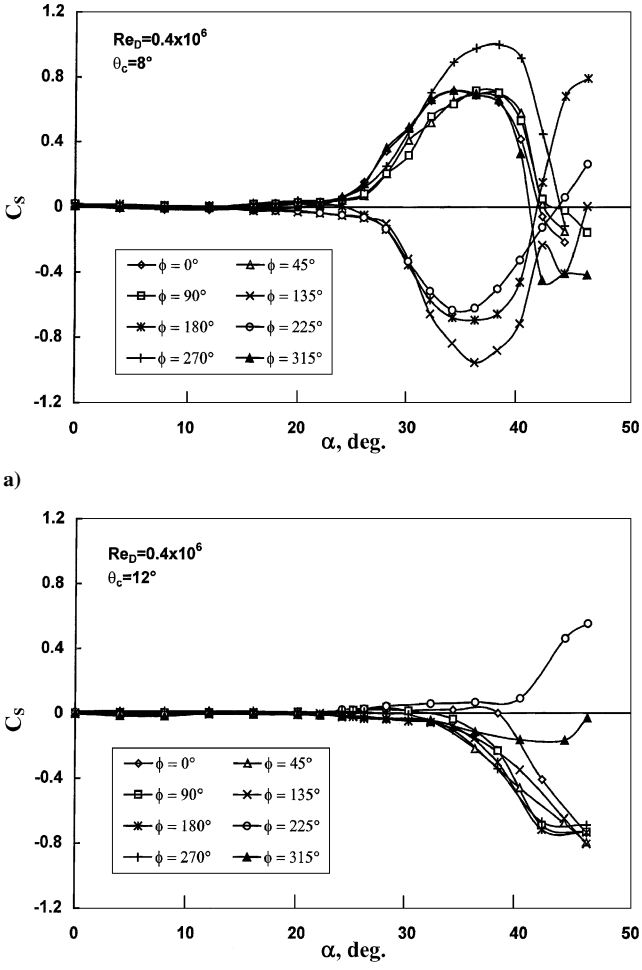

Fig. 5 Variation of side force with roll orientation for sharp cones.

1) Normal-force coefficient, $\Delta C_N \leq \pm 0.02 C_N$ (20 to 1).
2) Side-force coefficient, $\Delta C_s \leq \pm 0.02 C_s$ (20 to 1).
3) Static pressure coefficient, $\Delta C_p \leq \pm 0.015 C_p$ (20 to 1).

Results and Discussions

General

In the context of studies on vortex asymmetry on slender bodies at high angles of attack, it is useful and appropriate to recall the importance of roll search and the determination of stable roll position for each configuration (Ref. 1). Stable roll is generally defined as the roll position corresponding to which the side force is at a maximum and is insensitive to small changes in roll angle. In the literature, typically no more than from four to eight roll positions are tested for roll sensitivity due to practical difficulties. In the present study, stable roll was determined for the sharp as well as all of the blunted cones by measuring the forces and moments at low speeds. Corresponding to laminar crossflow separation on the models, which is usually associated with the highest side-force levels, eight roll positions for both the sharp cone as well as for the blunted cones from 0 to 360 deg were selected (on each model). Typical characteristics of side-force variations for two sharp cones at different roll orientations at $Re_D = 0.4 \times 10^6$ are shown in Fig. 5. Based on these results, $\phi = 270$ and 45 deg were chosen as stable roll positions for the 8- and 12-deg sharp cones, respectively; these correspond to the maximum side-force levels generated. Similarly, side-force variations for blunt cones, $2r_N/D = 7\%$ for the 8-deg cone and 9% for the 12-deg cone, respectively, are show in Fig. 6 as a function of roll orientation. Here, $\phi = 180$ and 0 deg were chosen as stable roll positions for the aforementioned blunt cones, respectively. The present results with nose blunting are, therefore, considered more reliable because the measurements have been made at the stable roll position on each blunted cone. As noted by Hunt,[1] earlier measurements with nose blunting (Fig. 1) did not involve roll search.

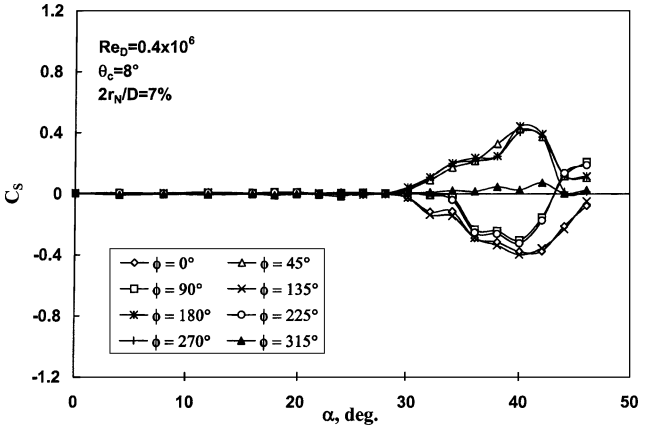

a)

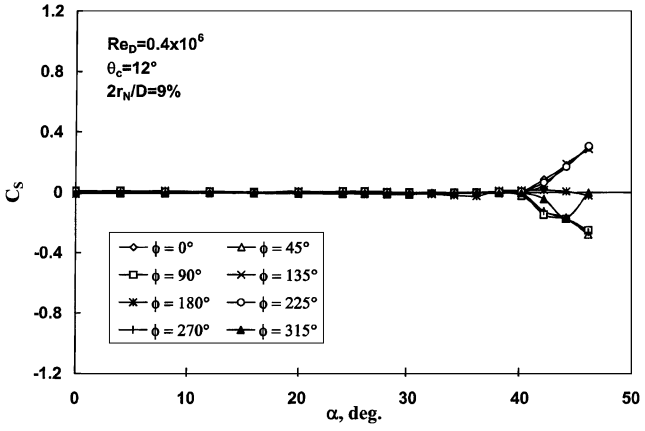

b)

Fig. 6 Variation of side force with roll orientation for blunt cones.

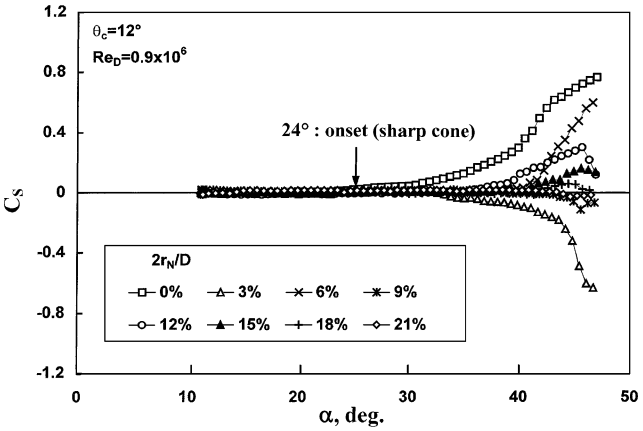

a)

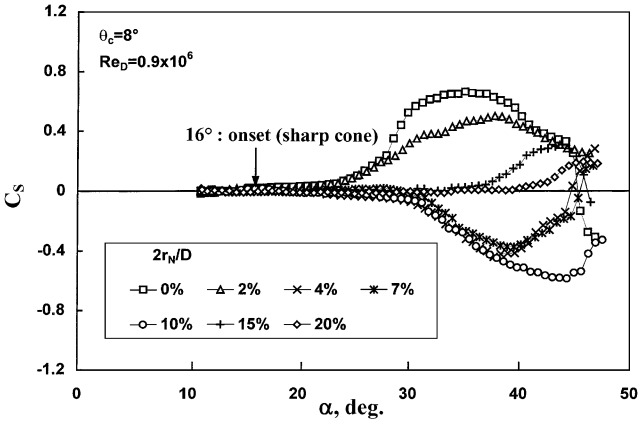

b)

Fig. 7 Side-force characteristics with nose blunting.

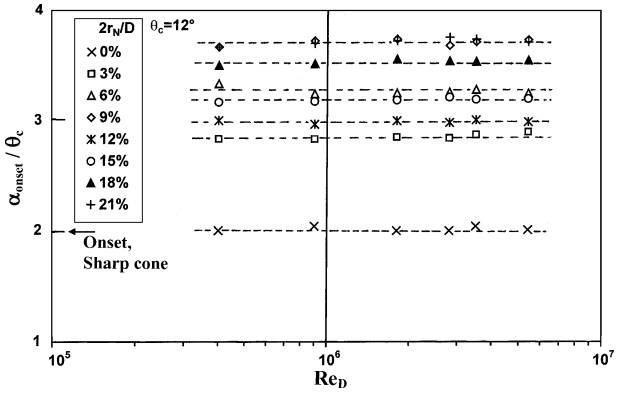

a)

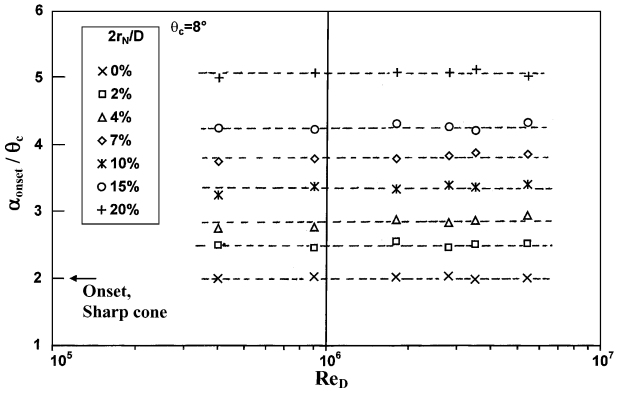

b)

Fig. 8 Effect of Reynolds number on vortex asymmetry onset.

Nose blunting brings in a new geometric parameter, namely, its diameter ($2r_N$), and it is not clear what would be an appropriate length scale for nondimensionalizing the nose radius. As in earlier studies,[5–8] we have adopted the base diameter D for normalizing the nose radius. (Although it is less relevant for this problem involving a nose triggered phenomenon.) Furthermore, it is convenient to use D, and, in addition, it has a constant value of 160 mm for all of the sharp and blunted models tested in the present experiments.

In what follows, we present primarily the characteristics of vortex asymmetry and induced side forces. The side force is nondimensionalized by the freestream dynamic pressure and reference area based on base diameter.

Typical results of side-force characteristics at a Reynolds number based on diameter Re_D of 0.9×10^6 for the 8- and 12-deg cones are shown in Fig. 7. For the sharp cones, the side force is the highest, and the onset angle for vortex asymmetry corresponds to nearly twice the semi-apex angle θ_c (a well-known feature for pointed forebodies[1]). Note that nose blunting results in a delay in the onset of vortex asymmetry and a decrease in side-force magnitudes as observed in some of the earlier studies.[5–8] It may also be inferred that the effectiveness of blunting in reducing the side-force magnitudes is nonmonotonic with bluntness ratio, as revealed in earlier observations (Fig. 1); this factor is discussed further in a subsequent section.

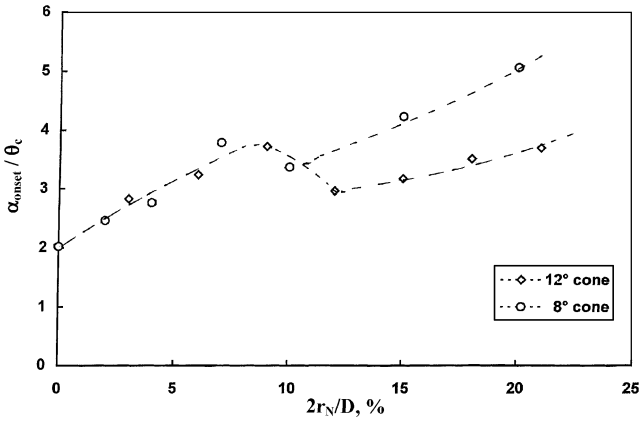

Fig. 9 Comparison of α_{onset} characteristics for the two blunted cone models.

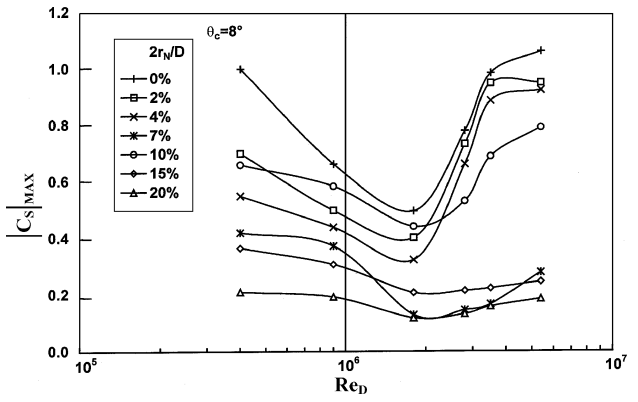

a) Variation of side-force characteristics with Reynolds number

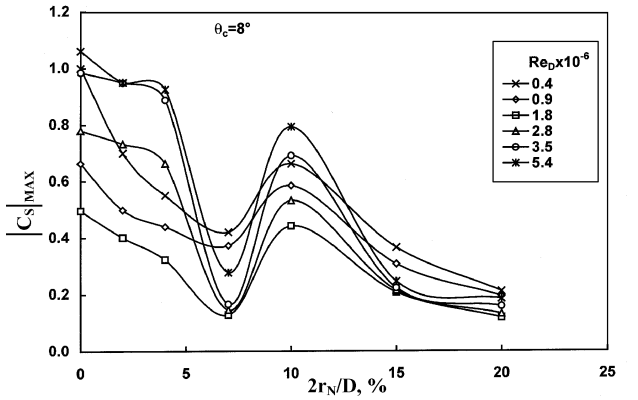

b) Variation of side-force characteristics with bluntness ratio

Fig. 10 Maximum side force characteristics on 8-deg cone model.

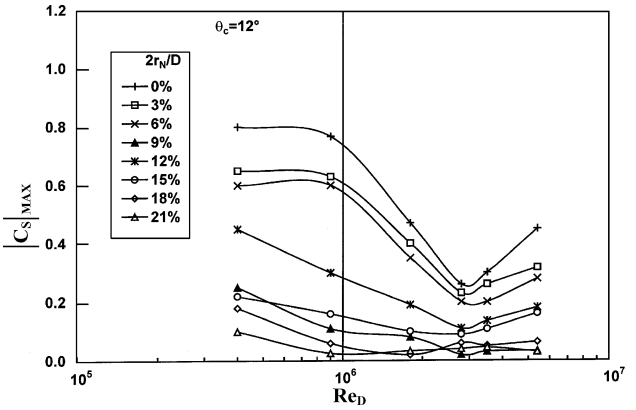

a) Variation of side-force characteristics with Reynolds number

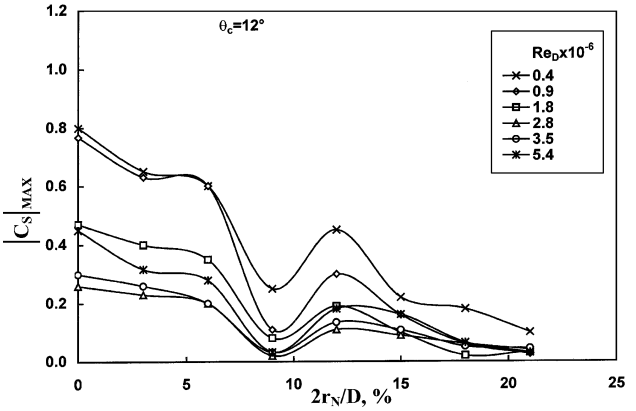

b) Variation of side-force characteristics with bluntness ratio

Fig. 11 Maximum side-force characteristics on 12-deg cone model.

Characteristics of Vortex Asymmetry Onset

Determination of the angle of attack for the onset of vortex asymmetry α_{onset} is an important aspect of the problem. In the present work, vortex asymmetry onset is identified as the angle of attack for which the side-force coefficient C_S is 0.02; this value was chosen because the balance system used could resolve the side-force coefficient to this accuracy reliably. The results of α_{onset} as dependent on Reynolds number Re_D for the sharp as well as for the blunted cones are presented in Figs. 8a and 8b for the 12- and 8-deg cones, respectively. In Figs. 8, α_{onset} is scaled by an appropriate value of θ_c of the sharp cone for the results on both the sharp as well as the blunt cones. Note that the surface slope of a blunted cone, downstream of nose blunting, has the same value as the θ_c of the sharp cone.

For the sharp cones, α_{onset} values correspond to $2\theta_c$, a well-known feature of pointed forebodies.[1] A remarkable feature of the results (Figs. 8a and 8b) is that α_{onset} on each blunted cone is also nearly independent of the freestream Reynolds number (within the accuracy of determination of α_{onset}, ± 1 deg) over a wide range of Re_D varied here. Also evident from Fig. 8 is that α_{onset}/θ_c increases initially up to a certain bluntness ratio ($2r_N/D$), decreases, and then shows an increase again for large values of $2r_N/D$. The preceding features of α_{onset} suggest an initial decrease in side-force levels up to a certain bluntness ratio, a reversal in side-force level, and a decrease for large bluntness ratios (to be discussed in the next section).

Figure 9 shows a superposition of the results of Figs. 8a and 8b for the cone models of 8 and 12 deg; we have shown the average

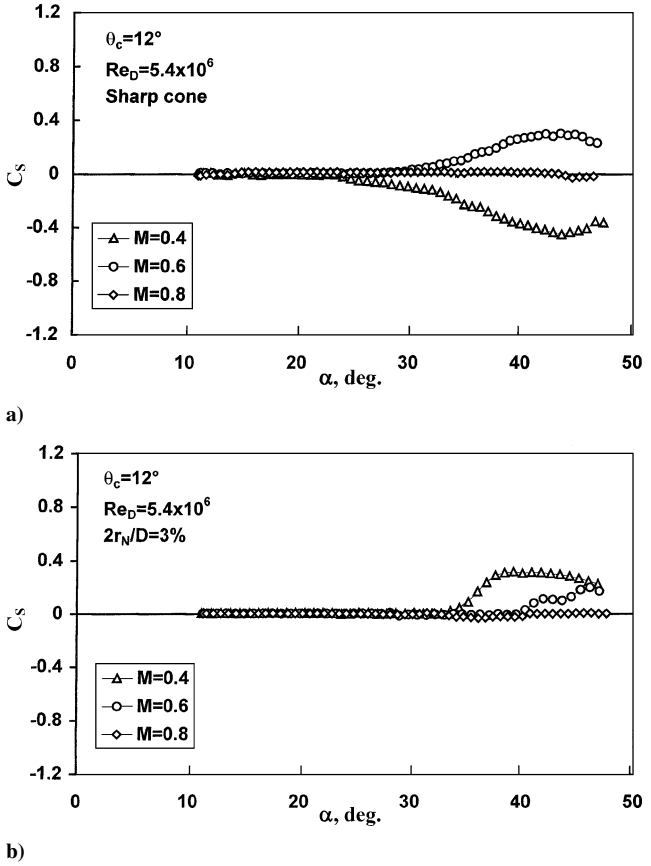

Fig. 12 Effect of Mach number on side-force characteristics.

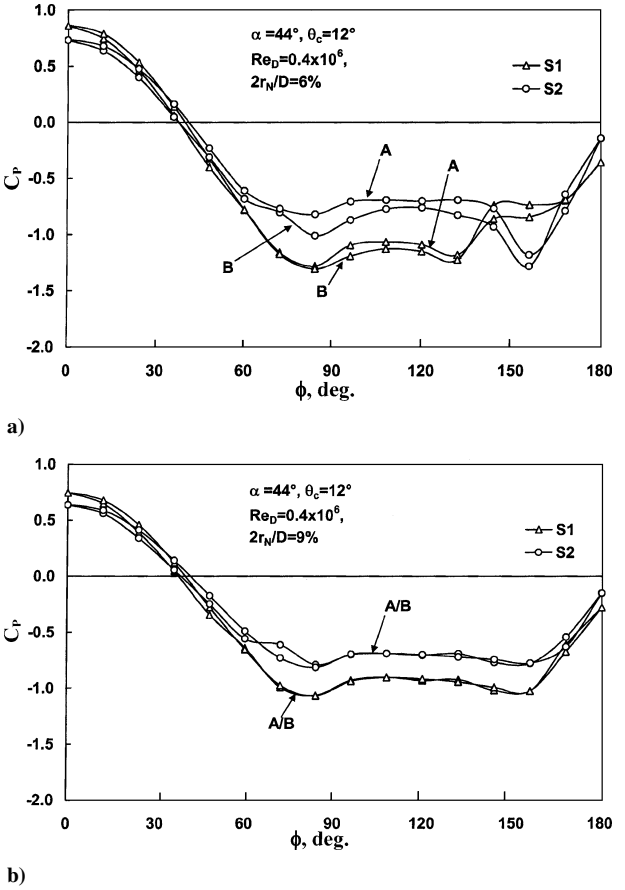

Fig. 14 Circumferencial pressure distributions on blunt cones.

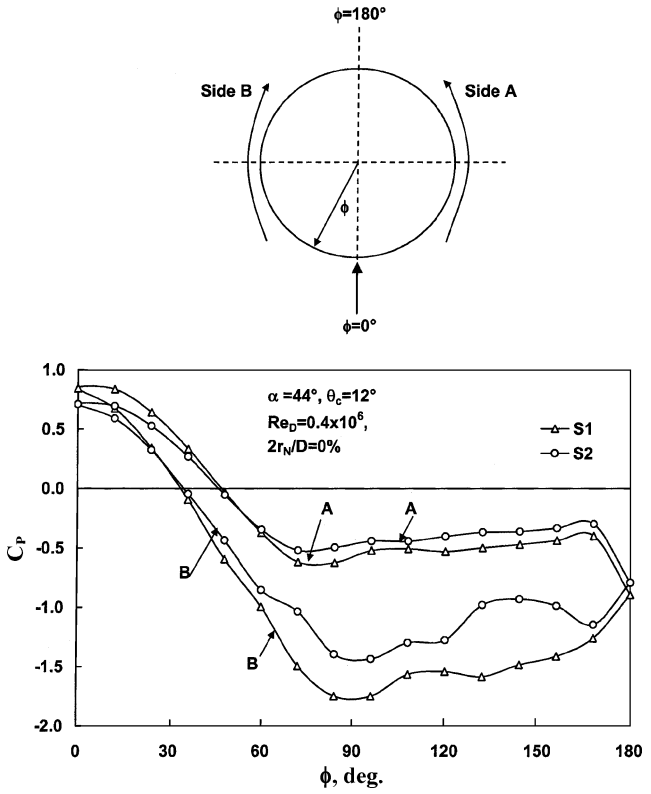

Fig. 13 Circumferencial pressure distributions on 24-deg sharp cone.

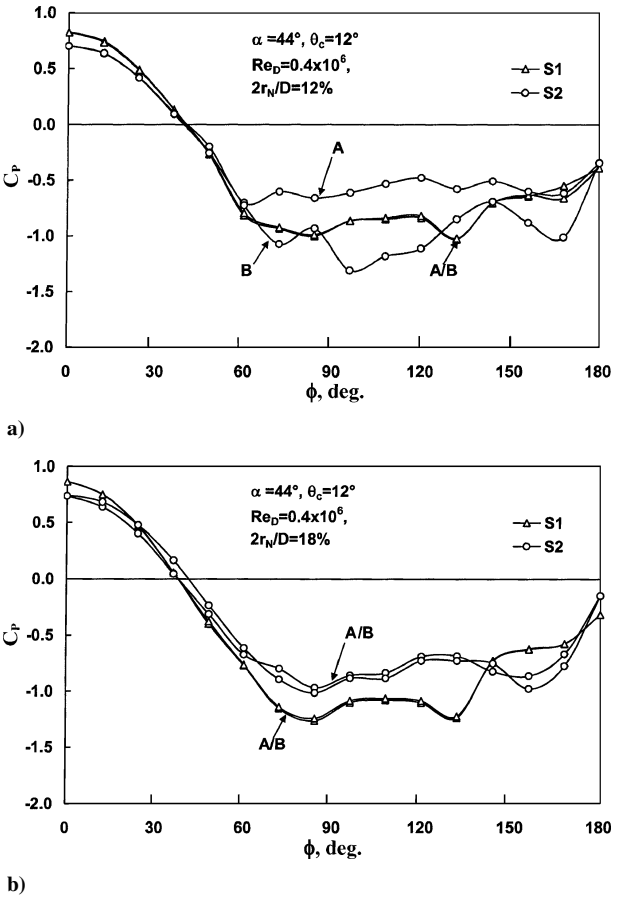

Fig. 15 Circumferencial pressure distributions on blunt cones.

value of α_{onset}/θ_c over the Reynolds number range in Fig. 9. Note that there is near collapse of the vortex asymmetry data up to a bluntness ratio of about 9%, beyond which there are differences for the two families of blunted cone models; the differences essentially seem to arise beyond the nose bluntness ratio corresponding to first side force minimum.

In Figs. 8 and 9, some of the interesting observations on vortex asymmetry on blunted cones have been presented. The α_{onset} characteristics on each blunted cone is virtually independent of freestream Reynolds number (over the range of Re_D examined), and, furthermore, a useful correlation for α_{onset} is suggested (Fig. 9) based on model geometrical parameters, namely, θ_c and D. It is indeed interesting that for both sharp as well as for blunt cones that α_{onset} correlates with geometrical parameters.

Side-Force Characteristics with Nose Blunting

The results of side-force characteristics obtained on all models have been analyzed, and the absolute values of maximum side force generated at each value of Re_D will be presented next. The results of side force are plotted against Re_D first and then cross plotted with nose bluntness ratio for the 8- and 12-deg cones in Figs. 10 and 11, respectively. The following major features may be noted:

1) For small bluntness ratios, the side force variation with Re_D is qualitatively similar to sharp cones (high in laminar and turbulent and low in transitional Reynolds numbers). As nose bluntness is further increased, the side-force variations nearly flatten off, exhibiting only a small variation with Re_D (Figs. 10a and 11a).

2) The side-force levels decrease initially up to a certain bluntness ratio and then increase and gradually decrease for large values of bluntness ratio (Figs. 10b and 11b). The rise in side-force levels beyond the first minimum is very dramatic for the 8-deg cone. Whereas the increase in side-force levels beyond the first minimum is qualitatively similar to those observed in earlier studies (Fig. 1), the present data definitely indicate that there is a progressive decrease in (maximum) side-force levels to relatively low values for large bluntness ratios. The results also show that the blunting is relatively more effective on the 12-deg cone in terms of minimum side-force levels reached; in fact, on the 8-deg cone, the maximum C_S value is still around 0.15 at a bluntness ratio of 20% (Fig. 10a).

3) The decrease or increase in side-force levels with nose blunting is associated with a corresponding increase or decrease, respectively, in α_{onset} values (Figs. 9–11).

4) The first minimum in (maximum) side force occurs at around 7 and 9% blunting for the 8- and 12-deg cones, respectively; these

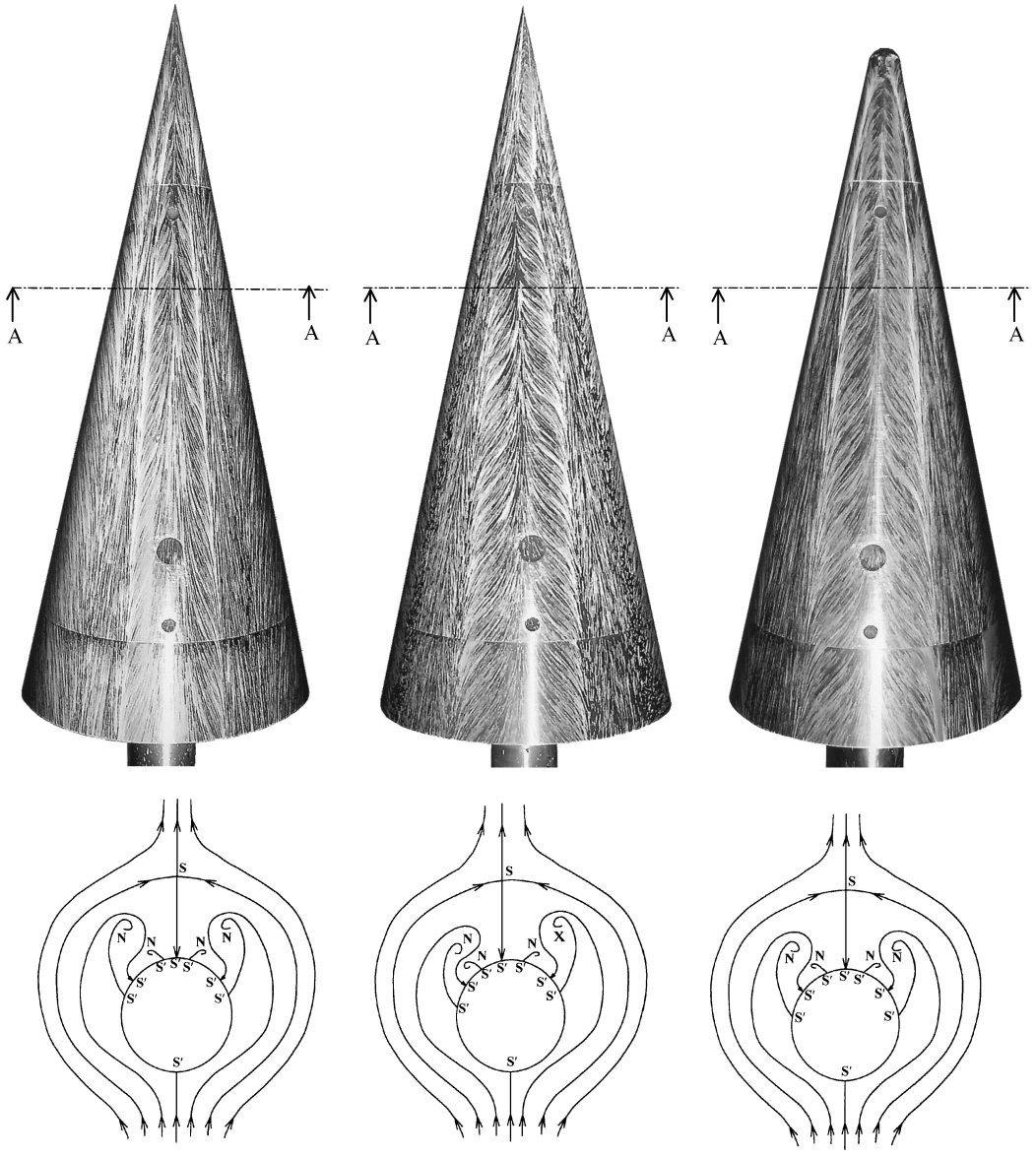

a) Symmetrical flow features, sharp cone, $\alpha = 23$ deg, $Re_D = 3.5 \times 10^6$

b) Asymmetrical flow features, sharp cone, $\alpha = 44$ deg, $Re_D = 3.5 \times 10^6$

c) Symmetrical flow features, blunt cone ($2r_N/D = 9\%$), $\alpha = 44$ deg, and $Re_D = 3.5 \times 10^6$

Fig. 16 Typical surface flow visualization photographs and crossflow streamlines on 12-deg cone model for *N*, node; *S*, saddle; and *S′*, half-saddle.

results are broadly similar to the results shown in Fig. 1. Also note that, for each case, the optimum bluntness ratio corresponding to the first minimum in C_S value is independent of Re_D over the range tested.

5) Interestingly, the minimum values of (maximum) C_S occur over the same range of Re_D for both sharp and blunted cones, for example, $Re_D \sim$ from 2.0×10^6 to 4.0×10^6 for the 12-deg cone).

Effect of Mach Number on Side-Force Characteristics

Mach number effects on side forces generated are shown for the 12-deg sharp cone and for a blunt cone of bluntness ratio ($2r_N/D$) of 3% at a fixed Re_D of 5.4×10^6 in Figs. 12a and 12b, respectively. For the sharp cone, an increase in Mach number delays the onset of vortex asymmetry progressively, and asymmetry is completely avoided up to an angle of incidence of 45 deg at $M = 0.8$ (Fig. 12a); these results due to compressibility effects are very similar to those observed on pointed forebodies.[1,6,8,22] Note in Fig. 12b that bluntness further delays the onset of vortex asymmetry to an angle of incidence of about 34 deg at $M = 0.4$ and 40 deg at $M = 0.6$, suggesting that bluntness is effective at higher Mach numbers as well. The results on the 8-deg cone were qualitatively similar to those obtained on the 12-deg cone.[23]

Surface Pressure Distributions

Surface pressure distributions were made on the 12-deg cone model at two longitudinal locations of 150 mm ($S1$) and 300 mm ($S2$) from the nose tip (Fig. 4). Typical results for a sharp and for blunted cones ($2r_N/D = 6$, 9, 12, and 18%) obtained at a speed of 40 m/s are shown in Figs. 13–15, revealing the effect of blunting on circumferencial pressure distribution. Note for the sharp cone (Fig. 13) that the pressure distributions on two sides of the cone are significantly different at both the $S1$ and $S2$ locations, giving rise to a large side force. Note that nose blunting progressively symmetrizes the pressure distributions starting from the nose region (Figs. 13–15). For example, for $2r_N/D = 6\%$ (Fig. 14a), the pressure distributions at $S1$ are nearly symmetric whereas some asymmetry remains at the $S2$ location, giving rise to a moderate side force. Furthermore, for $2r_N/D = 9\%$ (Fig. 14b), pressure distributions at $S1$ and $S2$ are virtually symmetric, leading to very low side-force levels as observed in balance measurements (Fig. 11b). The first rise in side force at $2r_N/D = 12\%$ is associated with asymmetry in pressure distribution at the $S2$ location (Fig. 15a). With a further increase in bluntness ($2r_N/D = 18\%$), pressure distributions become symmetric at both of the locations (Fig. 15b). Also note from the preceding results (Figs. 13–15) that, whereas asymmetry in pressure distribution exists virtually from the windward plane of symmetry ($\phi = 0$ deg, Fig. 13) for the sharp cone, it is significantly delayed ($\phi \approx 60$ deg, Figs. 14 and 15) on blunted cones.

Surface Flow Visualization

Typical surface flow visualization photographs on the sharp as well as on the blunted ($2r_N/D = 9\%$) 12-deg cone model at a Reynolds number of 3.5×10^6 are shown in Fig. 16; also shown are crossflow streamlines along section AA for the preceding cases, which are topologically consistent. Figure 16a shows symmetrical surface flow features at $\alpha = 23$ deg just before the onset of vortex asymmetry ($\alpha_{\text{onset}} = 24$ deg) and asymmetric features at $\alpha = 44$ deg (Fig. 16b), corresponding to high side-force levels (Fig. 7a) for the sharp cone. The blunted cone shows nearly symmetrical surface flow features (Fig. 16c) at $\alpha = 44$ deg, corresponding to the low side forces ($C_S = 0.05$, Fig. 11b) observed. It was difficult to infer details of surface flow features in the nose region due to the small physical dimensions of the model. Broadly similar flow features were observed on the 8-deg cone models as well.[23]

Conclusions

A detailed experimental investigation has been carried out for the first time to study the effect of nose bluntness on the characteristics of vortex asymmetry and induced side forces on slender cones at low speeds. In these tests, nose bluntness was systematically varied in the range from 0 to 20% based on base diameter, and measurements were made over a wide range of Reynolds numbers from 0.4×10^6 to 5.4×10^6 for two cone models of semi-apex angle of 8 and 12 deg. For each model configuration, roll search has been carried out, leading to the identification of stable roll position. Some of the major conclusions include the following:

1) The results show that (scaled) values of α_{onset} due to nose blunting are independent of Re_D within the Reynolds number range studied and that θ_c, the nose semi-apex angle, is a useful scaling parameter for α_{onset}. It is indeed interesting that the α_{onset} on blunt cones correlates with geometrical parameters. The optimum bluntness ratio corresponding to a first minimum in side force is again independent of Reynolds number on both cone models.

2) The side-force levels decrease initially up to a certain bluntness ratio, then increase, followed by a gradual decrease for large values of bluntness ratios; this decrease or increase in side-force levels with nose blunting is associated with a corresponding increase or decrease, respectively, in α_{onset} values. Analysis of surface pressure distributions suggest that nose blunting progressively symmetrizes the flow from the nose region to the rear end of the body.

3) Whereas the increase in side-force levels beyond the first minimum is qualitatively similar to those observed in earlier studies, the present data definitely indicate that there is a progressive decrease in side-force levels to relatively low values for large bluntness ratios, which could form an important input for design applications.

4) The results show that bluntness is relatively more effective on the 12-deg cone compared to the 8-deg cone. The minimum side-force level attained on the 8-deg cone has a value of about 0.15, suggesting that even at a large bluntness ratio (20%), asymmetry is not completely destroyed.

Acknowledgments

The authors sincerely thank the Aeronautical Development and Research Board, Government of India, for their financial assistance to carry out this work. Thanks are due to the staff of the 1.2-m trisonic wind tunnel and the 1.5-m low-speed wind tunnel for their valuable help during wind-tunnel testing.

References

[1] Hunt, B. L., "Asymmetric Vortex Forces and Wakes on Slender Bodies," AIAA Paper 82-1336, Aug. 1982.

[2] Ericsson, L. E., and Reding, J. P., *Asymmetric Flow Separation and Vortex Shedding on Bodies of Revolution*, Progress in Astronautics and Aeronautics, AIAA, Washington, DC, 1989, pp. 391–452.

[3] Champigny, P., "Side Forces at High Angles of Attack. Why, When, How?," La Recherche Aerospatiale, No. 4, 1994, pp. 269–282.

[4] Williams, D. R., "A Review of Forebody Vortex Control Scenarios," AIAA Paper 97-508, Feb. 1997.

[5] Chapman, G. T., Keener, E. R., and Malcolm, G., "Asymmetric Aerodynamic Forces on Aircraft Forebodies at High Angles of Attack—Some Design Guides," Paper 16, AGARD, Nov. 1976.

[6] Pick, G. S., "Investigation of Side Forces on Ogive–Cylinder Bodies at High Angles of Attack in the $M = 0.5$ to 1.1 Range," AIAA Paper 71-570, June 1971.

[7] Keener, E. R., Chapman, G. T., Cohen, L., and Talaghani, J., "Side Forces on a Tangent-Ogive Forebody with a Fineness Ratio of 3.5 at High Angles of Attack and Mach Numbers from 0.1 to 0.7," NASA TM X-3437, Feb. 1977.

[8] Keener, E. R., Chapman, G. T., Cohen, L., and Talaghani, J., "Side Forces on Forebodies at High Angles of Attack and Mach Numbers from 0.1 to 0.7. Two Tangent Ogives," NASA TM X-3438, Feb. 1977.

[9] Roos, F. W., and Magness, C. L., "Bluntness and Blowing for Flowfield Asymmetry Control on Slender Forebodies," AIAA Paper 93-3409, Aug. 1993.

[10] Malcolm, G. N., "Forebody Vortex Control: A Progress Review," AIAA Paper 93-3540, Aug. 1993.

[11] Yuan, C. C., and Howard, R. M., "Effect of Forebody Strakes on Missile Asymmetric Vortices," *Journal of Spacecraft and Rockets*, Vol. 28, No. 4, 1991, pp. 411–417.

[12] Modi, V. J., Cheng, C. W., Mak, A., and Yokomizo, T., "Reduction of the Side Force on Pointed Forebodies Through Add-On Tip Devices," *AIAA Journal*, Vol. 30, No. 10, 1992, pp. 2462–2468.

[13] Westmoreland, S., and Gebert, G., "Strake Effectiveness for Controlling Out-of-Plane Loading on Missile Configurations," AIAA Paper 2000-0386, Jan. 2000.

[14]Ng, T. T., and Malcolm, G. N., "Aerodynamic Control Using Forebody Strakes," AIAA Paper 91-618, Jan. 1991.

[15]Chen, L., Ng, T. T., and Smith, B., "Forebody Vortex Control Using Nose-Boom Strakes," *Journal of Aircraft*, Vol. 32, No. 4, 1995, pp. 896–898.

[16]Murri, D. G., and Rao, D. M., "Exploratory Studies of Actuated Forebody Strakes for Yaw Control at High Angles of Attack," AIAA Paper 87-2557, AIAA, 1987.

[17]Rao, D. M., "Side Force Alleviation on Slender Pointed Forebodies at High Angles of Attack," *Journal of Aircraft*, Vol. 16, No. 11, 1979, pp. 763–768.

[18]Lua, K. B., Lim, T. T., Luo, S. C., and Goh, E. K. R., "Helical Groove and Circular Trip Effects on Side Force," *Journal of Aircraft*, Vol. 37, No. 5, 2000, pp. 906–915.

[19]Fidler, J. E., "Active Control of Asymmetric Vortex Effects," *Journal of Aircraft*, Vol. 18, No. 4, 1981, pp. 267–272.

[20]Polhamus, E. C., "A Review of Some Reynolds Number Effects Related to Bodies at High Angles of Attack," NASA CR 3809, Aug. 1984.

[21]Kline, S. J., and McClintock, F. A., "Describing Uncertainties in Single-Sample Experiments," *Mechanical Engineering*, Vol. 75, No. 1, 1953, pp. 3–8.

[22]Viswanath, P. R., "Vortex Asymmetry and Induced Side Forces on Elliptic Cones at High Incidence, *Journal of Aircraft*, Vol. 32, No. 5, 1995, pp. 1018–1025.

[23]Kumar, R., and Viswanath, P. R., "Experimental Investigation of Side Force Control on Circular Cones Using Nose Blunting," National Aerospace Labs., Rept. PD NT 0315, Bangalore, India, May 2003.